AEROELASTIC DESIGN OF THE OLAF REFERENCE AIRCRAFT CONFIGURATION

Matthias Schulze[1], Thomas Klimmek[1],
Francesco Torrigiani[2], Tobias Wunderlich[3]

[1]DLR, Institute of Aeroelasticity (AE), Göttingen, Germany
[2]DLR, Institute of System Architecture in Aeronautics (SL), Hamburg, Germany
[3]DLR, Institute of Aerodynamics and Flow Technology (AS), Braunschweig, Germany

Abstract

One of the main aims of the EU Flightpath 2050 is to significantly reduce the fuel consumption of upcoming designs for transport aircraft. To achieve this challenging goal, new technologies have to be investigated. In this context, the development of the 'optimally load adaptive aircraft' (oLAF) for a conventional design is one of the main goals of the DLR project oLAF. Since the lift-to-drag ration, the structural mass and the thrust specific fuel consumption are the main drivers of the aircraft's fuel consumption, an improvement in all three topics seems to be a promising approach to fulfill the intended aims of the European Union. That's why the design of the new oLAF configuration is equipped with a next generation three shaft geared turbofan engine with an ultra-high bypass-ration and an optimized aerodynamic performance combined with aggressive load-alleviation (LA) techniques to lighten the load-carrying structure of the aircraft significantly compared to a conventional state-of-the-art aircraft. Multiple design cycles with different degree of fidelity and LA approaches are planned to be performed within oLAF. At the current state of the project, three different designs are available. On the one hand, there is the more basic configuration of the overall aircraft design (OAD) further called 'oLAF_SLv1'. On the other hand, there are configurations with more mature aerodynamic characteristics further called the 'oLAF_ASv0' configuration as start design for a multidisciplinary-design-optimization (MDO) process and the 'oLAF_ASv1' as the optimized result of the MDO. All configurations have been analyzed and evaluated using the aeroelastic structural design tool cpacs-MONA. The optimized oLAF_ASv1 configuration has furthermore been checked on aeroelastic stability. Conclusively, the stiffness of the structural pylon model has been adapted to shift a hump-mode of the new generation engine to higher airspeeds, so that the instability occurs outside of the flight envelope.

Keywords

cpacs-MONA; aeroelastic design; load alleviation; parametric modelling; OAD; MDO; oLAF; CPACS

1. INTRODUCTION

In a multi-fidelity aircraft design process, the first activity is the definition of an initial configuration starting from the top-level aircraft requirements (TLARs) using low-fidelity and handbook methods. The initial configuration is modified and refined by higher-fidelity methods and, if necessary, the same tools used to obtain the initial configuration are re-executed to propagate the high-fidelity results to every aircraft design area which is not covered by the high-fidelity process. This final step is called overall aircraft design (OAD) synthesis. In the HAP1 of the oLAF project both the OAD initialization and synthesis are carried out by DLR-SL in collaboration with DLR-AT which is providing the engine design. The XDSM graph in Figure 1 represents the workflow to obtain the oLAF_SLv1 configuration. The process consists of a single loop converging the maximum take-off mass (MTOM) and fuel mass. The two tools integrated in the workflow are OpenAD [1] and AMC.

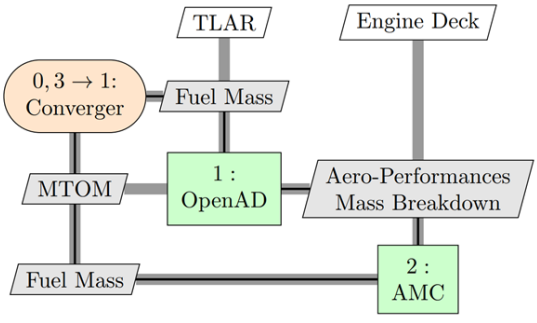

Figure 1. XDSM of the DLR-SL workflow used to obtain the oLAF_SLv1 configuration

OpenAD is an overall aircraft design tool developed at DLR-SL based on well-understood and mostly publicly available handbook methods. Starting from the TLARs (see Table 1) provided by DLR-AS, OpenAD is used to obtain the main geometrical parameters for the wing, fuselage, and tail planes, an initial mass-breakdown, a costs estimation and a simplified aerodynamic performance map.

Table 1. TLARS of the oLAF reference configuration

Aircraft Parameter	Value
OEM	118 t
MTOM	220 t
Max. payload	54 t
MMO	0.86

OpenAD has the additional functionality to generate a CPACS file. CPACS is the common parametric aircraft configuration schema developed by DLR [2] to enable large collaborative design workflows. The initial CPACS file contains the main design results and many other geometrical details (like the airfoils or the wing structural layout) which are not defined by OpenAD, but instead directly taken from similar aircraft configurations. The purpose is to reduce the integration effort for the higher-fidelity tools which do not need to generate the entire CPACS file from scratch but can directly update values in the schema or generate only a sub-part of it. AMC is a mission analysis tool which allows the computation of fuel consumption, required thrust, emissions and aircraft trim for each point of the mission trajectory. AMC is used to increase the accuracy of the fuel mission estimation done with OpenAD, exploiting the engine design capability provided by DLR-AT.

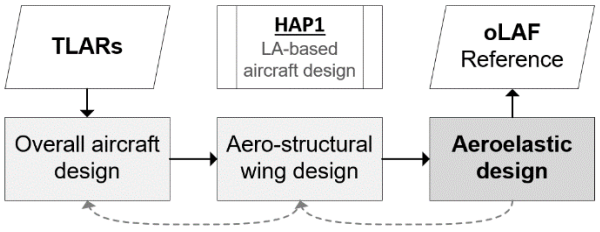

Figure 2. Simplified flow-chart of the HAP1 process to design the oLAF reference aircraft configuration

The next step in the multi-fidelity aircraft design process of oLAF's main work package one (HAP1) is the aero-structural wing design (see Figure 2). This optimization process is based on high fidelity simulation methods [3] and [4]. Based on the result of the OAD the parametric models for the aero-structural wing optimization are built. The outer shape of the fuselage and the belly fairing are derived from an existing CAD model. The wing planform of the baseline aircraft is introduced based on the wing area, aspect ratio and leading-edge sweep angle of the wing geometry developed with OpenAD. The wing is furthermore discretized into 16 wing sections and a winglet is added. To be able to perform reliable CFD-analysis, the more basic wing airfoils of the oLAF_SLv1 configuration are exchanged by the transonic airfoils and the outer shape of the NASA Common Research Model (CRM) [5]. Additionally, an ultra-high bypass-ratio three shaft geared turbofan engine of the next generation has been selected for the aircraft.

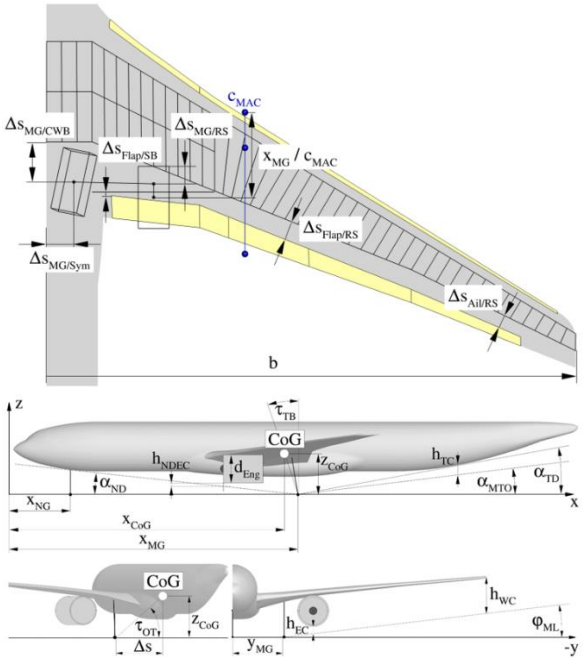

Figure 3. Geometrical constraints for the aero-structural wing design process

The geometrical constraints for the wing design consist of constraints for airport conformity and for the integration of the engine, the landing gear and the control surfaces. Figure 3 gives an overview of the parameters for the definition of the geometrical constraints, which have to be fulfilled for each wing design. This includes the positioning of the main gear wheel on the ground with a given relative x-position while maintaining the minimal allowed distances between the main landing gear, the control surfaces, and the wing box. Furthermore, the geometrical constraints for nose down engine clearance h_{NDEC}, touch down tail clearance h_{TC}, and engine h_{EC} and wing clearances h_{WC} for a bank angle of $\rho=5°$ have to be fulfilled. All geometrical constraints are checked for each prescribed position, until a feasible design is found.

The objective function of the multi-mission aero-structural wing optimization is the combined fuel consumption of three selected flight missions. Thereby, the fuel consumption is defined in terms of fuel burn per range and payload. Hence, the combined fuel consumption is the weighted sum of the corresponding mission fuel consumption.

After the aero-structural wing design of the oLAF HAP1, the aeroelastic design and assessment is performed using cpacs-MONA [6]. cpacs-MONA is an automatized aeroelastic structural design tool developed at DLR-AE in Göttingen. Within this tool three main steps are conducted. The parametric model set-up using the DLR-AE in-house model generator ModGen [7], followed by an extensive loads analysis campaign of the flexible aircraft structure and a structural optimization of the wing-like structures taking aeroelastic requirements like sufficient control surface efficiency into account. ModGen sets up all FE-models for the loads analysis and for the component wise structural optimization. All simulations are performed using the FE-analysis software MSC Nastran [8]. cpacs-MONA can be used as a stand-alone tool (like for the HAP1 process) or as part of various aircraft design processes like high-fidelity MDO chains [9], [10], [11]. cpacs-MONA is built modular and is written in Python code. It extracts the information about the aircraft from a CPACS-dataset. cpacs-MONA automatically reads out the information about the wing planform, the wing topology like rib and spar positions, and initial component thicknesses together with the engine, pylon, and landing gear locations and dimensions. It also uses information about aircraft masses like design, primary and secondary masses plus the dimensions of the control surfaces, and the borders of the fuel tanks. For this paper over 1000 load cases according to CS25.335 [12] containing symmetrical pull-up and push-down maneuvers, yawing and rolling maneuvers paired with dynamic gust encounters are calculated for each aircraft configuration with six different mass cases. For the pull-up and push-down maneuvers, the ailerons are symmetrically deflected proportional to the dynamic pressure to alleviate the maximum loads [13]. The optimization model consists of the definition of design variables, constraints, and an objective function. The objective function for the structural optimization is to minimize the wing-box mass under consideration of aeroelastic constraints like control surface efficiency or allowable strain values per shell element. As design variable the thickness of the shell elements for the load-carrying wing structures can be adjusted to fulfill the objective function. The design variables are combined to design regions to minimize the optimization task. The loads analysis and the structural optimization are iteratively coupled, while the mass and the stiffness of the simulation models are updated at each step until the mass and the loads of the aircraft configuration are converged. At the end of the convergence loop, additional analysis can be performed within cpacs-MONA according to the purpose of the output of the process.

2. AIRCRAFT CONFIGURATIONS

For this paper, three different aircraft configurations have been analyzed. The pre-design of the OAD named oLAF_SLv1, the MDO start design oLAF_ASv0 and the optimized oLAF_ASv1. Each configuration will be presented separately in the following paragraphs. First of all, an overview over the twist distribution and the planform of the three configurations is given. In Figure 4, the spanwise twist distribution of the main wing is presented. It can be seen, that the aerodynamic characteristic of the basic oLAF_SLv1 is more elementary than the ones from the aerodynamic configurations. The twist of the OAD design is monotonously decreasing from root to tip but is positive over the whole span, while the MDO start configuration has a so-called S-twist with negative values at 50 percent of the span and at the tip region. The optimizer of the MDO process has lifted the twist of the oLAF_ASv0 to only have a negative value at the tip of the wing.

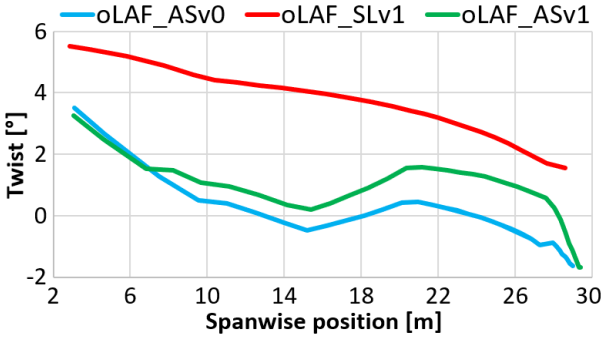

Figure 4. Spanwise twist distribution of the three investigated configurations

2.1. Overall aircraft design (oLAF_SLv1)

At the beginning of the oLAF project, the OAD-team in Hamburg (DLR-SL) sets up a CPACS-dataset using its tool OpenAD to fulfill the desired TLARS as depicted in Table 1. In a CPACS-dataset almost all aircraft parameters like geometry, structure,

materials, masses, etc. can be defined. At this state, handbook formulations are used to estimate the aircraft component masses. A more elementary structural definition regarding rib-layout, the material definition or the aerodynamic characteristic is stored within the CPACS-dataset coming from the OAD. The resulting OAD-configuration is furthermore called oLAF_SLv1. The GFEM/Dynamic of the oLAF_SLv1 as output of cpacs-MONA is highlighted in Figure 5. GFEM stands for global finite element model, and dynamic expresses the applicability of the model for structural dynamic analysis.

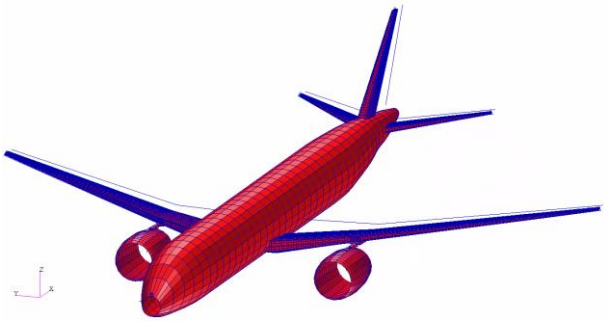

Figure 5. GFEM/Dynamic of the oLAF_SLv1 configuration

Table 2 shows the design parameters of the oLAF_SLv1 together with similar aircraft configurations: The Airbus research model XRF1, a long-range wide body transport aircraft developed by Airbus as part of the eXternal Research Forum (XRF) and the commercial Airbus A350-900.

Table 2. oLAF_SLv1 design parameters in comparison with reference aircraft configurations

Design Parameter	oLAF SLv1	XRF1	A350-900	Unit
Design range	6000	5500	8100	nm
Des. payload	31.0	38.5	-	t
Design Mach	0.83	0.83	0.85	-
Max Range	8276	9557	-	nm
MTOM	220	245	280	t
OEM	117	132	145	t
Wing loading	656	655	633	kg/m^2
Wing area	334	374	442	m^2
Wing span	57.7	60.9	64.8	m
Wing AR	9.92	9.91	9.49	-

The maximum take-off mass (MTOM) of *220 t* is in line with the reference configurations considering the different payload and range requirements. The mass-breakdown for the MTOM and the operating empty mass (OEM) is illustrated in Figure 6.

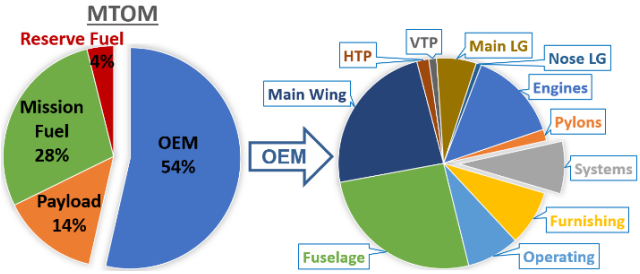

Figure 6. Mass-breakdown of the MTOM and the OEM of the oLAF reference configuration

Within the OEM of *117 t*, the wing mass is *28 t*, the fuselage structural mass is *30 t* and the total on-board systems mass is *9.4 t* accounting respectively for *26%*, *28%* and *9%* of the OEM. The design mission with a range of *6000 nm* and a payload of *31 t* has an initial cruise altitude of *34000 ft* and a final cruise altitude of *40000 ft*. The maximum thrust in cruise is *131 kN* and the cruise lift-to-drag ratio varies between *18.3* and *19.1*. The obtained payload range diagram at design Mach number is presented in in Figure 7, together with the payload-range of the two reference configurations.

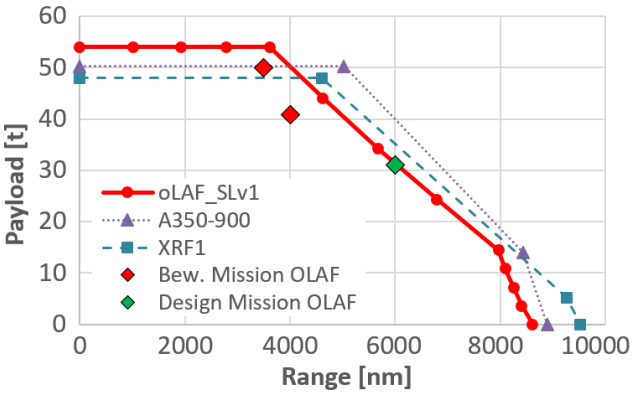

Figure 7. Payload-range diagram for the oLAF configuration at *Ma=0.83* and the reference aircraft

All the above results refer to the initial configuration for the HAP1 of the oLAF project. In the next iteration the synthesis capability will be used to integrate the higher fidelity results in the overall aircraft design process.

2.2. MDO start design (oLAF_ASv0)

The team of the aerodynamic-experts in Braunschweig (DLR-AS) modified the low-fidelity design coming from the OAD and enhance it by introducing more aerodynamic performance driving profiles and twist distribution based on previous wing planform optimization results [4] forming the hi-fi oLAF_ASv0 MDO start configuration. As mentioned in Paragraph 1, the aero-structural design process

has detailed geometrical constraints concerning the integration of the engine and the landing gear to the wing. To find a feasible MDO start design, the positioning of the wing, the inboard sweep angle and the inboard and outboard dihedral angles have been modified on the basis of the oLAF_SLv1 geometry. The span has been increased and a winglet has been introduced at the wing-tip. The resulting wing geometry for all three designs is shown in Figure 8 and their main wing parameters are listed in Table 3.

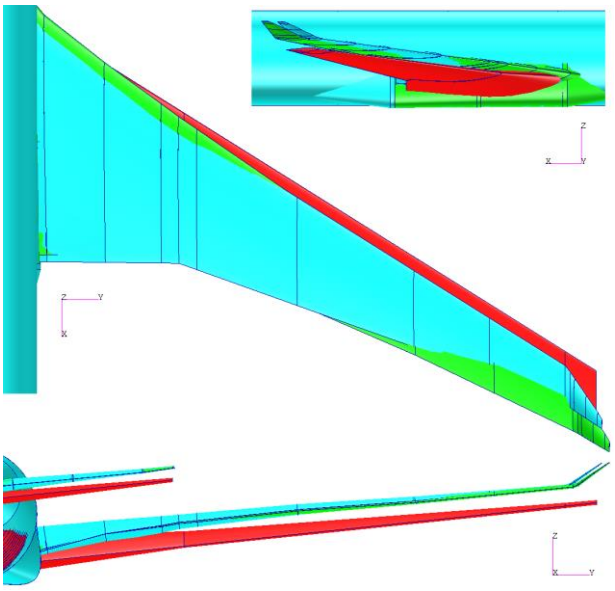

Figure 8. Wing planform overview of the three investigated configurations

Figure 9 visualizes the GFEM/Dynamic of the oLAF_ASv0 and Figure 10 shows an exploded view of the main wing to outline the topology of the load carrying structure for the oLAF_SLv1 in comparison to the oLAF_ASv0 MDO initial design.

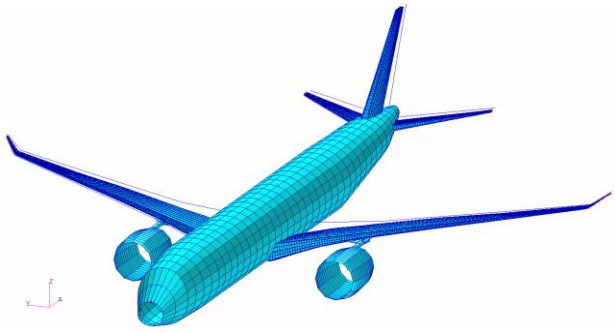

Figure 9. GFEM/Dynamic of the oLAF_ASv0 configuration

The main wing topology of the oLAF_SLv1 contains 39 ribs and two spars. The components skin, ribs and spar webs are made out of aluminum. For the oLAF_ASv0, these components are made out of composite material, and a mid-spar has been introduced into the model for a better introduction of the engine inertia loads. The wing of the oLAF_ASv0 furthermore contains seven more ribs, whereas six ribs are placed at the winglet device.

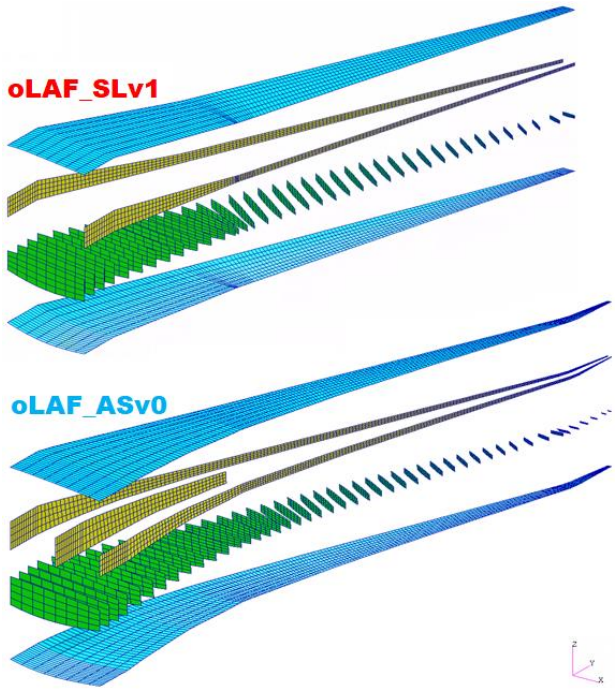

Figure 10. Exploded view of the main wing for the comparison of the wing topology for the oLAF_SLv1 (top) and the oLAF_ASv0 (bottom) configurations

2.3. MDO optimum design (oLAF_ASv1)

The result of the aero-structural wing optimization, the oLAF_ASv1 configuration, shows a wing with a slightly increased aspect ratio, an increased outboard sweep angle and a significant thin inboard wing compared to the initial oLAF_ASv0 design. Figure 11 represents the considerable decrease of the optimized wing thickness over the dimensionless span-coordinate η. The height of the mid spar at the root section of the wing decreases from *1.62 m* for the oLAF_ASv0 design to *1.36 m* for the optimum wing of the oLAF_ASv1.

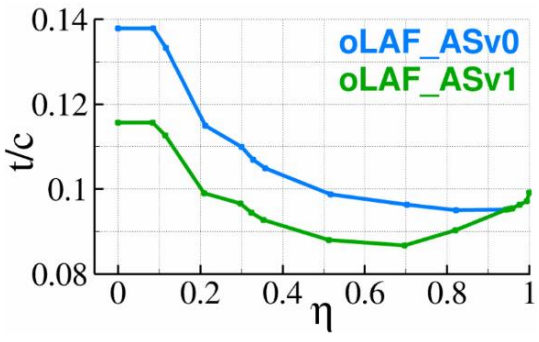

Figure 11. Airfoil thickness distribution for the main wing of the two AS configurations

With the aero-structural wing optimization an optimal trade-off between cruise flight performance and wing mass in terms of combined fuel consumption has been achieved. This leads to improved cruise flight performance without drawbacks due to wing mass changes. The corresponding cruise flight performance in terms of lift-to-drag ratios is increased substantially. Due to the wing optimization a reduction of the fuel consumption in the order of seven percent has been achieved. The result of this wing optimization represents the basis for the aeroelastic design part within the oLAF HAP1 process. Table 3 lists the main wing parameters of the three investigated configurations together with the from the sub-tools estimated operating empty masses (OEM_{CPACS}).

Table 3. Main aircraft (A/C) parameters of the three investigated configurations

A/C parameter	oLAF SLv1	oLAF ASv0	oLAF ASv1
Wing area	335 m^2	339 m^2	339 m^2
Wing span	57.7 m	58.2 m	58.9 m
Aspect ratio	9.9	10.0	10.2
MAC	7.0 m	7.7 m	7.6 m
LE Sweep	32.0°	35.3°	36.9°
OEM_{CPACS}	117.2 t	115.8 t	117.0 t

3. RESULTS OF THE AEROELASTIC DESIGN

The three afore presented configurations have been analyzed using the aeroelastic structural design tool cpacs-MONA. A special attention will be turned on the dimensioning load cases of the different configurations, the resulting mass of the wing structure together with the components structural thickness distribution. As a result of the thickness and planform of the designs, the influence on the structural elasticity and the aeroelastic stability will also be presented within the following paragraph.

3.1. Dimensioning load cases

To reduce the computational effort of the optimization task within cpacs-MONA, a component-wise load case selection is performed. Within this selection, a convex hull is placed over pairs of cutting loads for the shear forces, the bending and torsional moments forming the so-called loads envelope for a selected number of monitoring stations. The forces and moments of these load cases are extracted and used for the structural optimization of the wing-like components.

Table 4. Maxima cutting loads of the wing root bending moment ($Mx_{y=0}$) and wing root torsional moment ($My_{y=0}$) of the three configurations

Unit: [Nm]	oLAF SLv1	oLAF ASv0	oLAF ASv1
max. $Mx_{y=0}$	$2.14x10^7$	**$2.32x10^7$**	$2.28x10^7$
min. $Mx_{y=0}$	$-7.17x10^6$	**$-7.91x10^6$**	$-7.74x10^6$
max. $My_{y=0}$	$2.01x10^6$	$2.13x10^6$	**$2.24x10^6$**
min. $My_{y=0}$	$-8.55x10^6$	$-8.92x10^6$	**$-9.38x10^6$**

Table 4 lists the maximum and minimum cutting loads of the wing root bending moment and torsional moment for the three investigated designs. It can be seen, that the maxima bending moments occur at the oLAF_ASv0 configuration while the maxima torsional moments occur at the oLAF_ASv1 configuration due to the higher sweep angle.

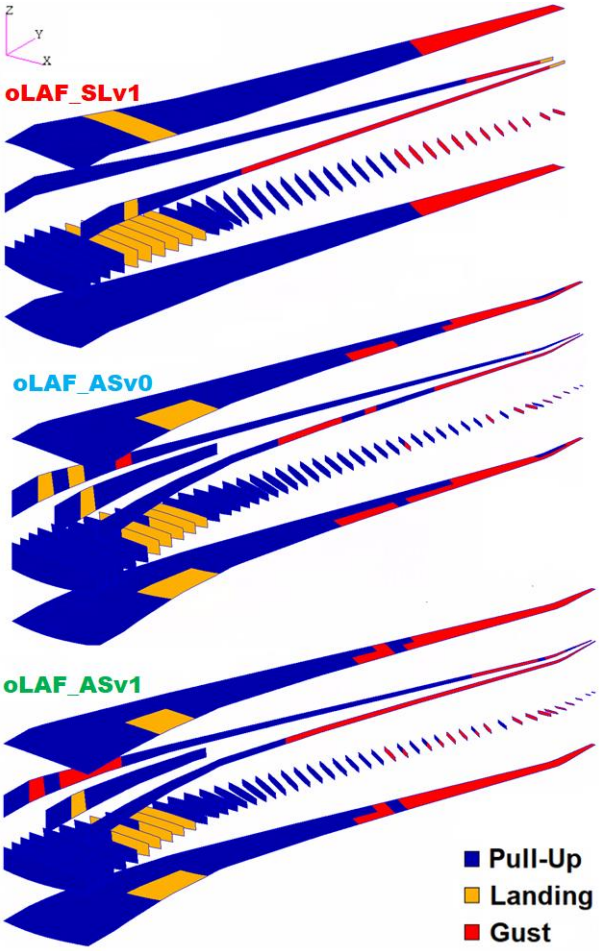

Figure 12. Dimensioning load case types for the main wing of the three configurations

Figure 12 illustrates, what kind of load case leads to the maximum loads at a specific component and region of the wing. The distribution of dimensioning load cases looks similar for all three configurations. The gust loads are dominant at the wing-tip, while

the 2.5g pull-up maneuvers are dominating the majority of wing. The conceptual ground and landing loads lead to the maximum loads at the region, where the landing gear is attached to the wing. Due to the thinner wing of the optimized oLAF_ASv1 configuration, the gust loads are higher at the engine, what can be seen due to the larger red areas at the front spar, where the engine is attached to the wing.
Another point to highlight at Figure 12 is the discretization of the design fields. At the MDO configurations, where three spars are integrated at the wing, the ribs are divided into two sub-ribs, while the ribs of the OAD design have one design field per rib. The design fields for the upper and lower skin are also divided into two fields in chordwise direction while the OAD design has just one design field between two neighboring ribs.

3.2. Wing primary mass

An important result of the aeroelastic design process for the OAD synthesis is the resulting optimized wing mass for the different aircraft to update the results coming from the OAD. Table 5 itemizes the resulting masses for the main wing, the horizontal (HTP) and the vertical tail-plane (VTP) and the consequent operating empty mass. It can be seen, that the OAD wing mass (CPACS) is *1.9 t* lighter than the mass coming from the aeroelastic design (oLAF_SLv1), while the masses for the tail-planes decrease. That leads to a *1.1 t* difference between the OEM coming from the simplified OAD methods and the physics-based methods within cpacs-MONA. A comparison of the oLAF_SLv1 and the oLAF_ASv0 design shows, that the new wing design with a more realistic twist distribution together with the new airfoils and the change from metal to composite lead to a mass reduction of *4.6 t* for the main wing. The optimized MDO configuration oLAF_ASv1 has an increase of wing mass of *1.5 t* compared to the initial MDO design. The reason for this increase of mass is explained in the following subchapter.

Table 5. Operating empty and wing mass of the OAD and the results of cpacs-MONA

Mass item	OAD *(CPACS)*	oLAF SLv1	oLAF ASv0	oLAF ASv1
OEM	117.2 t	118.3 t	114.7 t	116.3 t
Wing	27.9 t	29.8 t	25.2 t	26.7 t
HTP	2.16 t	1.64 t	1.65 t	1.62 t
VTP	1.40 t	1.11 t	0.97 t	0.98 t

3.3. Wing structural component thickness

Since the maximum take-off mass for the different designs is the same, their maximum loads are comparable (see Table 4), especially for the oLAF_ASv0 and the oLAF_ASv1 design with a likewise planform. The in Paragraph 3.2 mentioned increase in wing mass for the optimized design can be explained with the decrease of the wing thickness due to the optimized airfoils (Paragraph 2.3). Since the wing-box ribs and spars of the optimized wing have less design height but similar loads, the structural thickness of the load-carrying structure has to be increased to withstand the loads. A comparison of the structural thickness distribution for the wing-box components of the two MDO main wings can be seen at Figure 13. It is clearly evident, that the structural thickness of the optimized oLAF_ASv1 wing is increased at the region of the landing gear and the engine attachment. Within the structural optimization of the oLAF_ASv0 wing-box, only a few design fields reached the upper bound of the design space (*30 mm*), while the oLAF_ASv1 wing has a large region of maximum thickness, especially at the lower skin surface between the landing gear and the engine attachment.

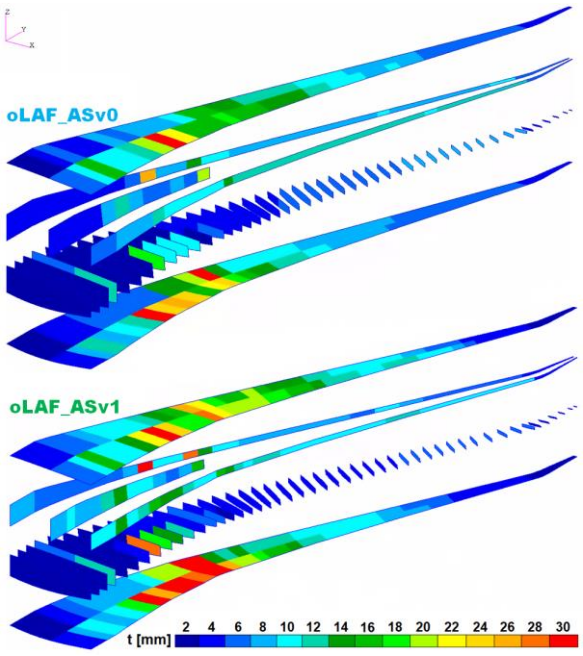

Figure 13. Structural thickness distribution of the main wing components for the two AS configurations

3.4. Wing structural elasticity

The displacement of the wing in flight and maneuver state is a first indicator for the structural elasticity of the aircraft´s wing. Figure 14 visualizes the displacement of the three investigated configurations

under a level flight-load (left) and under a 2.5g pull-up maneuver (right). The lowest translational z-displacement (T3) occur at the oLAF_SLv1 design and the highest at the optimized oLAF_ASv1.

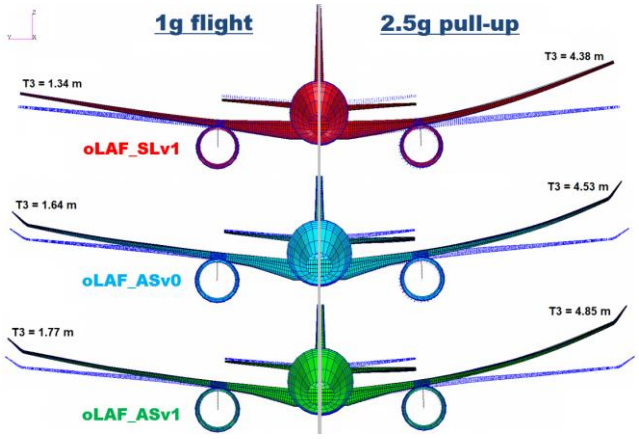

Figure 14. Displacements of the main wing for all configurations under 1g (left) and 2.5g loads (right)

Figure 15 shows the first symmetric wing bending mode shape and the corresponding eigenfrequency for the three investigated configurations. The eigenfrequency of the first symmetric wing bending mode (mode 7, mode 1-6 are rigid body modes) of the empty airplane is a next indicator for the structural elasticity of the aircraft´s main wing.

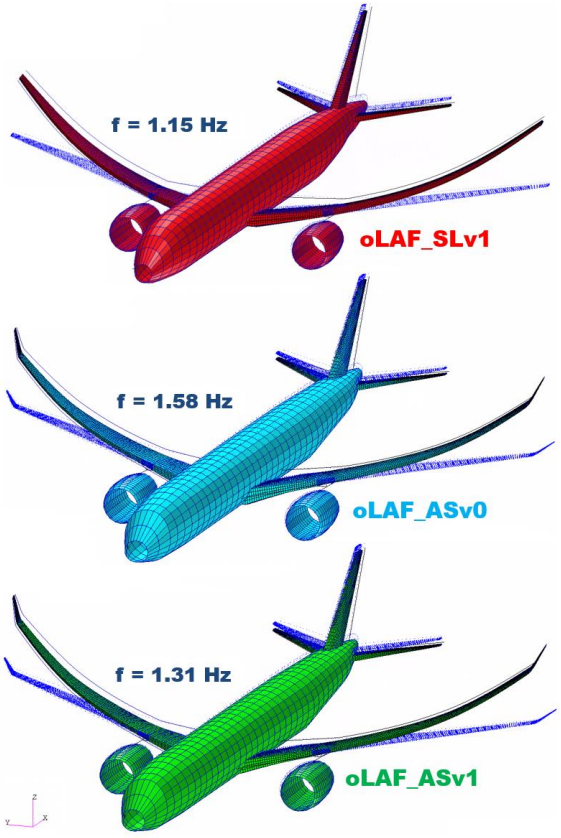

Figure 15. 1st symmetric wing bending mode of the OEM case of the three configurations

The oLAF_SLv1 configuration has the lowest first eigenfrequency while the highest occurs at the oLAF_ASv0. That the first elastic eigenfrequency of the initial MDO design is much higher than for the OAD configuration can be explained due to the stiffening effect of the introduced mid-spar and the different material of the load-carrying structural components of the wing. Since the wing of the optimized oLAF_ASv1 wing is much thinner than the initial MDO wing, its decrease in the first eigenfrequency can be explained.

3.5. Flutter check of the oLAF_ASv1

To make sure, that the oLAF reference configuration does not have an aeroelastic instability within the flight envelope, a transonic flutter check using MSC Nastran's Solution 145 [14] is performed at the end of cpacs-MONA for all six mass cases of the design. The non-matched flutter analysis using the *p-k-Method* with fixed Mach and fixed density is used. The Mach number is set to *0.8* and the density according to the international standard atmosphere to *0.525 kg/m³* for the flight level of *8000 m*.

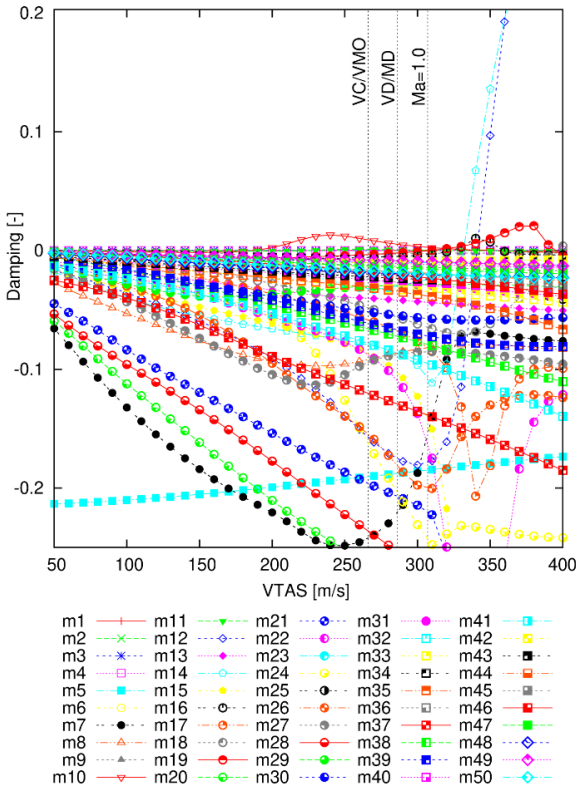

Figure 16. Flutter curves for the first 50 eigenmodes of the initial oLAF_ASv1 *MCRUI* configuration

For the cruise mass case (*'MCRUI'*) with full payload and 25 percent of the maximum fuel in the wing-tanks, a so-called hump-mode occurs, where for instance flutter appears in a limited velocity range

with moderate excitation, while the damping is recovering again for higher airspeeds. Figure 16 shows the flutter curves, aerodynamic damping over the true airspeed (*VTAS*), for the first 50 eigenmodes of the 'initial' oLAF_ASv1 configuration with pre-defined pylon parameters according to previous analyzed aircraft configurations within cpacs-MONA. For this pre-defined pylon parameters, the mode 10 (red triangle) shows the hump-mode with a positive aerodynamic damping starting at *200 m/s*. This behavior can be mainly observed for vibration modes where engines or control surfaces contribute. By taking a closer look into the mode shapes of the 'initial' oLAF_ASv1 design, it is noticeable, that three engine modes lie under two hertz (within the first five elastic eigenmodes). This indicates, that the pre-defined parameters for the structural pylon build with ModGen might be too flexible for the new generation ultra-high bypass-ratio engine. Figure 17 emphasis the feature of the pylon model of the GFEM/Dynamic for realistic eigenmodes of the pylon/engine.

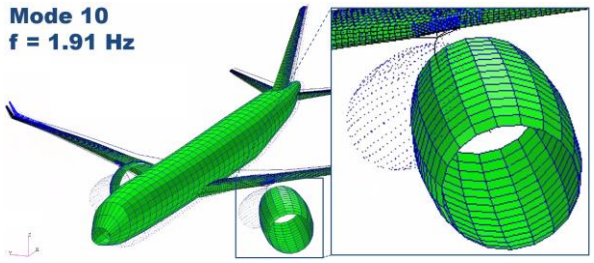

Figure 17. Mode shape 10 of the 'initial' oLAF_ASv1 configuration highlighting the elastic pylon model

Figure 18 visualizes the parametric model of the structural pylon for a wing mounted engine within ModGen. To shift the eigenfrequencies of the engine modes to higher frequencies and consequently the hump-mode to higher velocities, the parameters *PARH1* and *PARH2* have been increased to stiffen the pylon. For more details on the parametric modeling for the wing integration of the engine and pylon within cpacs-MONA, see [15].

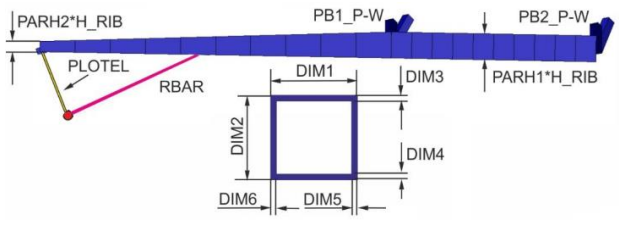

Figure 18. Visualization of the parameters for the structural pylon modelling

In Figure 19, the mode shapes of the eigenmodes 9 to 12 for the 'final' oLAF_ASv1 configuration with adapted pylon parameters is presented. With the new and stiffer pylon of the 'final' configuration, the engine eigenfrequencies are increased and the modes are shifted, with the result that no engine eigenmode occur under two hertz and only two modes occur under three hertz.

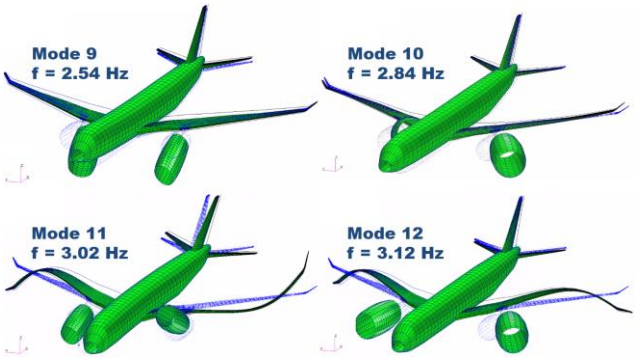

Figure 19. Mode shapes 9 to 12 of the 'final' oLAF_ASv1 configuration

Finally, the influence of the new pylon parameters on the flutter behavior of the 'final' oLAF_ASv1 configuration is presented in Figure 20. The stiffer pylon shifted the hump-mode to higher velocities, so that it starts to appear at dive-speed (V_D/M_D). A negative side-effect of the stiffer pylon is, that the slope of the damping-progression for the hump-mode steepened, and the hump becomes higher, leading to more intense flutter excitations.

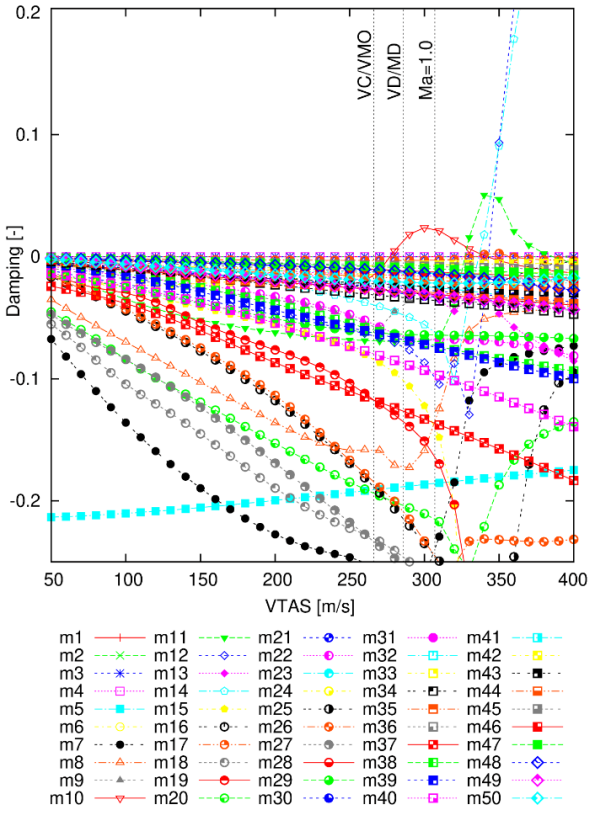

Figure 20. Flutter curves for the first 50 eigenmodes of the 'final' oLAF_ASv1 configuration

4. CONLUSIONS AND OUTLOOK

Within this publication, the oLAF HAP1 process and its sub-tools to develop the optimally load adaptive aircraft has been highlighted. The so far developed designs to form the oLAF reference aircraft configuration have been shown, starting from scratch with the OAD design oLAF_SLv1, followed by the MDO starting design oLAF_ASv0 and concluding with the MDO optimum design oLAF_ASv1. All the yet involved sub-processes and the differences in the derived designs have been introduced. A special attention has been turned on the results of the aeroelastic structural design process cpacs-MONA. cpacs-MONA has been used to analyze and evaluate the three aircraft designs to point out the influence of the different levels of fidelity regarding the loads, the structural optimization and the structural dynamic behavior. Conclusively, the influence of the pylon stiffness on the flutter characteristic of the optimized oLAF reference configuration has been demonstrated. By easily adapting some parameters of the elastic pylon model within cpacs-MONA, a hump-mode could be shifted to higher airspeeds, so that it occurs outside the elastic flight envelope of the aircraft.

One next step within the phase one of the HAP1 process will be the transfer of the with cpacs-MONA generated GFEM/Dynamic model for the optimized oLAF_ASv1 configuration to the colleagues of the DLR Institutes SR and FT, both responsible for the controlled loads- and gust-alleviation, to perform an enhanced load analysis campaign of the complete aircraft. In addition to that, the calculated loads of the cpacs-MONA process will be transferred to the colleagues from DLR-FA, as expert on the composite material design, to perform a more reliable lamination parameter optimization. After the reference configuration has passed the sequential design process of HAP1 twice, new developed load-alleviation techniques of the HAP2 will be introduces into the sub-processes of HAP1 to finally design the optimally load adaptive aircraft.

Bibliography

[1] S. Wöhler, G. Atanasov, D. Silberhorn and B. Fröhler, "Preliminary Aircraft Design within a Multi-disciplinary and Multi-fidelity Design Environment," in *Aerospace Europe Conference*, Bordeaux, France, 2020.

[2] M. Alder, E. Moerland, J. Jepsen and B. Nagel, "Recent Advances in Establishing a Common Language for Aircraft Design with CPACS," in *Aerospace Europe Conference*, Bordeaux, France, 25. - 28. Feb. 2020.

[3] T. F. Wunderlich and L. Reimer, "Integrated Process Chain for Aerostructural Wing Optimization and Application to an NLF Forward Swept Wing," in *Springer International Publishing*, Vol. 138, AeroStruct: Enable and Learn How to Integrate Flexibility in Design, 2018, pp. 3-33.

[4] T. F. Wunderlich, S. Dähne, L. Reimer, A. Schuster and O. Brodersen, "Global Aero-Structural Design Optimization of More Flexible Wings for Commercial Aircraf," in *AIAA Aviation Forum (virtual)*, 2020.

[5] J. C. Vassberg, M. Dehaan, M. Rivers and R. Wahls, "Development of a Common Research Model for Applied CFD Validation Studies," in *26th AIAA Applied Aerodynamics Conference, AIAA 2008-6919*, Honolulu, Hawaii, Aug. 2008.

[6] T. Klimmek, M. Schulze, M. Abu-Zurayk, C. Ilic and A. Merle, "cpacs-MONA – An Independent and in High-Fidelity Based MDO Tasks Integrated Process for the Structural and Aeroelastic Design of Aircraft Configurations," in *IFASD*, Savannah, USA, 2019.

[7] T. Klimmek, "Parametrization of Topology and Geometry for the Multidisciplinary Optimization of Wing Structures," in *European Air and Space Conference*, 2009.

[8] MSC Software Corporation, MSC Nastran 2021 Quick Reference Guide, United States of America: HEXAGON, 8. Dec. 2020.

[9] S. Görtz, C. Ilic, J. Jepsen, M. Leitner, M. Schulze, A. Schuster, J. Scherer, R.-G. Becker, S. Zur and M. Petsch, "Multi-Level MDO of a Long-Range Transport Aircraft Using a Distributed Analysis Framework," in *AIAA*, Denver, Colorado, USA, 2017.

[10] S. Görtz, M. Abu-Zurayk, C. Ilic, T. F. Wunderlich, M. Schulze, C. Kaiser, Ö. Süelözgen, A. Schuster, S. Dähne, M. Petsch, J. Häßy, S. Gottfried, R. Mischke, P. Knechtges and J. Hartmann, "Collaborative high fidelity and high performance computing-based MDO strategies applied to transport aircraft design," in *2nd European Workshop on MDO for Industrial Applications in Aeronautics*, Toulouse, France, 2019.

[11] M. Abu-Zurayk, A. Merle, C. Ilic, S. Keye, S. Görtz, M. Schulze, T. Klimmek, C. Kaiser, D. Quero-Martin, J. u. B. R. Häßy, B. Fröhler and J. Hartmann, "Sensitivity-based Multifidelity Multidisciplinary Optimization of a Powered Aircraft Subject to a Comprehensive Set of Loads," in *AIAA Aviation (virtual)*, 2020.

[12] F. A. Administration, *Federal Aviation Regulations Part 25 C, Airworthiness Standards: Transport Category Airplanes,* 2010.

[13] V. Handojo, *Contribution to Load Alleviation in Aircraft Pre-design and Its Influence on Structural Mass and Fatigue,* Technische Universität Berlin: Dissertation, 2020.

[14] MSC Software Corporation, MSC Nastran 2021 Aeroelastic Analysis User's Guide, United States of America: HEXAGON, 27. Nov. 2020.

[15] M. Schulze, J. Neumann and T. Klimmek, "Parametric Modelling of a Long-Range Aircraft under Consideration of Engine-Wing Integration," *Aerospace,* Vols. Special Issue Aeroelasticity, Volume II, pp. 8(1), 2, 2021.

Corresponding author: matthias.schulze@dlr.de